JACS
JOURNAL OF THE AMERICAN CHEMICAL SOCIETY
Communication
pubs.acs.org/JACS

Enhancing Perovskite Electrocatalysis through Strain Tuning of the Oxygen Deficiency

Jonathan R. Petrie,[†] Hyoungjeen Jeen,[†] Sara C. Barron,[‡] Tricia L. Meyer,[†] and Ho Nyung Lee*[,†]

[†]Materials Science and Technology Division, Oak Ridge National Laboratory, Oak Ridge, Tennessee 37831, United States
[‡]National Institute of Standards and Technology, 100 Bureau Drive, Gaithersburg, Maryland 20899, United States

Supporting Information

ABSTRACT: Oxygen vacancies in transition-metal oxides facilitate catalysis critical for energy storage and generation. However, promoting vacancies at the lower temperatures required for operation in devices such as metal−air batteries and portable fuel cells has proven elusive. Here we used thin films of perovskite-based strontium cobaltite ($SrCoO_x$) to show that epitaxial strain is a powerful tool for manipulating the oxygen content under conditions consistent with the oxygen evolution reaction, yielding increasingly oxygen-deficient states in an environment where the cobaltite would normally be fully oxidized. The additional oxygen vacancies created through tensile strain enhance the cobaltite's catalytic activity toward this important reaction by over an order of magnitude, equaling that of precious-metal catalysts, including IrO_2. Our findings demonstrate that strain in these oxides can dictate the oxygen stoichiometry independent of ambient conditions, allowing unprecedented control over oxygen vacancies essential in catalysis near room temperature.

Incremental changes in oxygen vacancies have leveraged large shifts in the electrocatalytic properties of transition-metal oxides (TMOs).[1] As a result of the catalytic effect of these oxygen deficiencies, changes in oxygen stoichiometry within binary oxides such as TiO_2 are known to affect water splitting and the oxygen evolution reaction (OER), which are important for energy production and storage devices, including photocatalysis, metal−air batteries, and fuel cells.[2,3] In addition to binary oxides, studies of more complex oxides, such as $CaMnO_{2.5}$ by Kim et al.,[4] have also suggested that oxygen vacancies near the surface can affect catalysis because of an increase in the number of active sites around these defects,[5] a weaker metal−oxygen bond yielding faster intermediate exchange,[6] and vacancy-induced electron doping that changes the spin configuration to e_g^1 for more efficient electron transfer.[7] Moreover, control of the oxygen anion concentration, rather than the metal cation concentration, minimizes the impurity and defect segregation complexities associated with heterovalent cation doping.[6a,8]

However, the highly oxidizing conditions associated with the OER limit the ability to retain oxygen deficiencies for such electrocatalysis. To truly functionalize the catalytic potential of oxygen vacancies in TMOs, a new parameter is required to allow control over the oxygen stoichiometry in surroundings that would normally suppress oxygen deficiencies. We recently used epitaxial thin films of strontium cobaltite ($SrCoO_x$, SCO) to demonstrate a relationship between strain and oxygen content in aprotic annealing environments of several hundred degrees Celsius.[9] This oxide has a topotactic transition between the brownmillerite phase, $SrCoO_{2.5}$ (BM-SCO), and the oxidized perovskite phase, $SrCoO_{3-\delta}$ with $0 \leq \delta \leq 0.25$ (P-SCO).[9b,c] As a result of the easy intercalation of O^{2-} through BM-SCO offered by its open framework and the metastability of Co^{4+} in P-SCO, SCO has an exceptionally low oxygen activation energy (<1 eV) that changes by tenths of an electron volt under strain.[10] Because of this intriguing blend of facile oxygen incorporation and oxygen activity, SCO was seen as an ideal candidate for examining the catalytic possibilities of strain-induced oxygen deficiencies in TMOs.

In this work, we used epitaxial strain engineering to systematically tune the oxygen stoichiometry of P-SCO thin films under conditions consistent with the critically important OER.[11] Without such strain, the highly oxidizing environment during the OER results in fully oxidized P-SCO with few vacancies.[12] After validation of a strain-induced change in oxygen stoichiometry both in the bulk and near the surface, we then used this control over the oxygen content to artificially augment the oxygen vacancies in P-SCO, yielding significantly enhanced OER activities. These activities compare favorably to that of a thin film of IrO_2 tested under the same conditions, demonstrating the promise of this method.

To monitor topotactic oxidation to P-SCO under OER conditions, a set of preoxidized BM-SCO films were epitaxially grown on lattice-mismatched substrates using pulsed laser epitaxy. These films had uniform film thicknesses of 15 nm to ensure minimal strain relaxation on various perovskite substrates. The substrates included (001) $(LaAlO_3)_{0.3}$-$(SrAl_{0.5}Ta_{0.5}O_3)_{0.7}$ (LSAT), (001) $SrTiO_3$ (STO), (110) $DyScO_3$ (DSO), (110) $GdScO_3$ (GSO), and (001) $KTaO_3$ (KTO), whose pseudocubic parameter (a_{sub}) varied from 3.868 to 3.989 Å. While BM-SCO is orthorhombic (a_0 = 5.574 Å, b_0 = 5.447 Å, c_0 = 15.745 Å), stoichiometric P-SCO is cubic with a_c = 3.829 Å, leading to substrate-induced tensile strains (ε) from 1.0 to 4.2% for fully oxidized SCO. The substrates were attached to glassy carbon (GC) rods. All of the films included a 10 nm thick $La_{0.8}Sr_{0.2}MnO_3$ (LSMO) conducting underlayer to ensure uniform charge transport from the rod to the cobaltite layer on nonconducting substrates.[13] In addition to its known inactivity in the OER,[13] the conducting LSMO allowed us to

Received: April 12, 2016
Published: May 27, 2016

DOI: 10.1021/jacs.6b03520
J. Am. Chem. Soc. 2016, 138, 7252−7255

eliminate the carbon binder used in other thin-film studies, which under testing may introduce an additional current due to carbon degradation or hybridization.[14] BM-SCO films were initially topotactically oxidized to P-SCO through ex-situ electrochemical oxidation for 5 min at 1.6 V vs RHE in a fully oxygenated 0.1 M KOH solution, which is consistent with OER conditions and has been shown to fully oxidize unstrained SCO.[12,15] Subsequent potentiodynamic and galvanostatic anodization scans confirmed the OER activity and a measure of stability, respectively (see the Supporting Information). X-ray diffraction (XRD) reciprocal space maps (RSMs) substantiated that after oxidation from BM-SCO, all of the P-SCO films on the aforementioned substrates were coherently strained in-plane (Figures S1 and S2), leaving the out-of-plane c parameter as the only free structural variable.

Figure 1a shows a representative XRD θ–2θ scan around the P-SCO 002 peak for both preoxidized BM-SCO and electro-

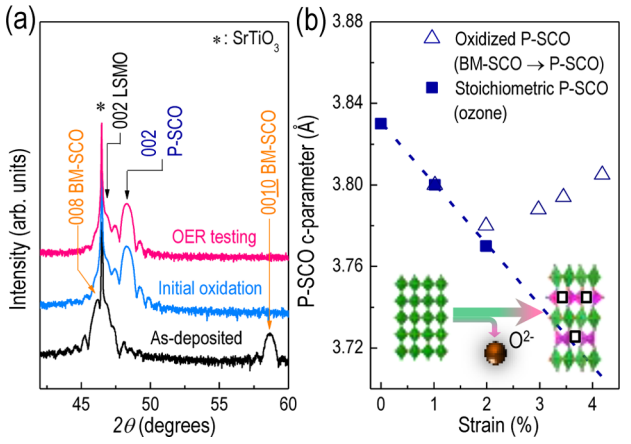

Figure 1. (a) Representative XRD θ–2θ scans of an as-deposited BM-SCO/LSMO film and an electrochemically oxidized P-SCO/LSMO film on a (001) STO substrate. The scans after the initial oxidation at 1.6 V for 5 min and post-OER testing are shown. (b) Deviation of the out-of-plane c parameter from the stoichiometric Poisson ratio of ~0.26 is due to oxygen vacancy formation. These vacancies can be found in oxygen-deficient layers (pink) that alternate with fully oxidized octahedral layers (green).

chemically oxidized P-SCO on an STO substrate (ε = 2.0%). The initial oxidation for 5 min at 1.6 V is displayed, as well as the same P-SCO film after OER activity and stability testing. All of the peaks are clearly defined with Kiessig fringes that verify the superior film quality and provide a measure of thickness. While the LSMO 008 peak shows no change after oxidation, the lack of both BM-SCO 002 and half-order 00$\underline{10}$ peaks indicates full conversion to P-SCO ($\delta \leq 0.25$) in all of the films. Along with no change in the X-ray reflectivity (not shown), the similarity between the P-SCO both before (initial oxidation) and after OER testing suggests that amorphization and degradation throughout the entire film did not occur. In Figure 1b, a plot of the P-SCO c parameter versus strain is compared to results from previous bulk (unstrained) P-SCO studies or prior studies on ozone-deposited P-SCO.[9a,b,12,15] In those studies, the P-SCO was nearly fully stoichiometric, and there was a clear linear shift in the c parameter that can attributed to a Poisson-type contraction with a ratio $\nu \sim 0.26$. However, the monotonic shift in the c parameter for our coherently deposited, electrochemically oxidized films increasingly diverges from this stoichiometric behavior with tensile strain $\varepsilon > 1\%$. Since an increase in the number of oxygen vacancies is known to result in lattice expansion for perovskite-type oxides, this uniaxial divergence in the only unconstrained direction (c parameter) is attributed to an increase in the number of oxygen deficiencies throughout the film.[16] As the tensile strain on the SCO film intensifies from ε = 1.0 to 4.2%, the increasing difference from the stoichiometric behavior signifies an increase in the number of oxygen vacancies.

Direct-current electrical transport measurements at room temperature (Figure 2a) also support this systematic change in

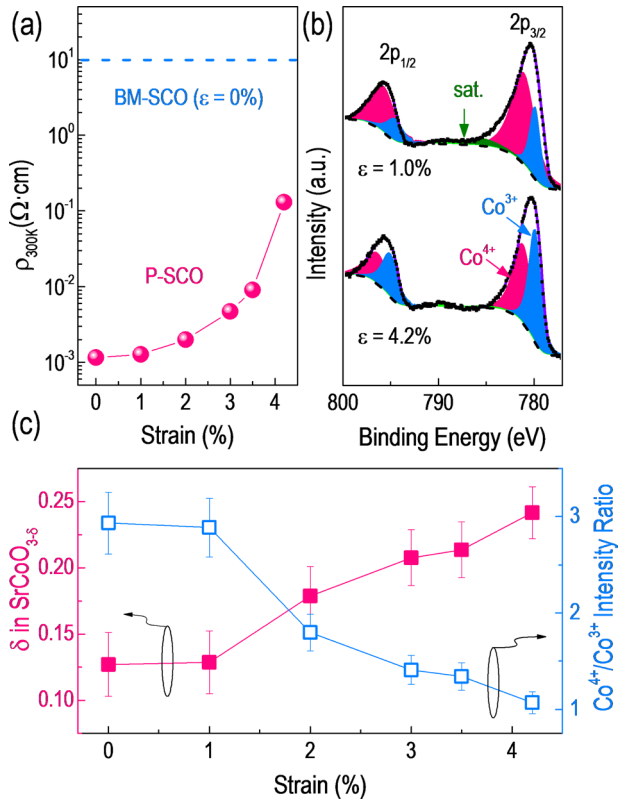

Figure 2. (a) Increase in the resistivity of strained P-SCO films at room temperature due to strain-induced loss of oxygen. (b) XPS Co 2p and satellite (sat.) peaks of electrochemically oxidized P-SCO on LSAT (ε = 1.0%) and KTO (ε = 4.2%) substrates. The fit is shown in purple. (c) Plot of the ratio of the intensities of the Co^{4+} and Co^{3+} peaks showing a clear trend toward decreasing Co valency with tensile strain, with a matching trend in oxygen nonstoichiometry (δ). A strain-relaxed P-SCO film on LSAO (ε = 0%) was used.

stoichiometry for $\varepsilon > 1\%$. A 15 nm thick strain-relaxed P-SCO film on $SrLaAlO_4$ (LSAO) was used as an unstrained control (ε = 0%). As the tensile strain increases, the film becomes less conducting, suggesting a higher concentration of oxygen vacancies.[9c] Indeed, for the resistivity over the 5–300 K temperature regime (Figure S3), only the strained film with $\varepsilon \leq$ 1% displays metallicity ($\delta \sim 0.1$); the ε = 1% film again shows similar properties to the unstrained film, and the others are not metallic because of vacancy-induced disruption of the exchange responsible for such behavior in fully oxygenated P-SCO.[9b] However, none of the films display the high resistivities typically found in a BM-SCO film of comparable thickness, putting an upper boundary on the oxygen deficiency at $\delta \leq 0.25$ for P-SCO.[17]

To further verify the change in oxygen content near the potentially catalytic surface, we investigated the strained P-SCO

DOI: 10.1021/jacs.6b03520
J. Am. Chem. Soc. 2016, 138, 7252–7255

films via X-ray photoelectron spectroscopy (XPS) using the Co 2p peaks. The oxygen stoichiometry was estimated by charge-compensating oxygen loss with a lower Co oxidation state.[9c] As expected from the XRD and electronic transport data, the unstrained P-SCO displays a spectrum similar to that of the ε = 1.0% film. As shown for the spectra of the ε = 1.0 and 4.2% films in Figure 2a, the shoulders at higher energies decrease with a greater degree of tensile strain, indicting spectral weight transfer from the fully oxidized Co^{4+} peak to the lower-energy Co^{3+} peak. Satellites related to the shake-up structure are also included. The shift in Co valency can be quantified via the intensity ratio of the Co^{4+} and Co^{3+} peaks, which falls from ~3 to ~1 between the minimum and maximum tensile strains (Figure 2b). Between the ε = 1.0 and 4.2% films, we can estimate an increase of $0.3e^-$, which is compatible with $\Delta\delta \leq 0.15$ in $SrCoO_{3-\delta}$ as the equilibrium state transitions from $SrCoO_{2.9}$ to $SrCoO_{2.75}$ with tensile strain.

Electrochemical tests, including *iR*-corrected cyclic voltammograms (CVs), galvanostatic anodization, and polarization curves, were performed to probe the oxidation of strained SCO and its OER activity as well as its stability under OER conditions. Figure 3a shows representative peaks from CVs of

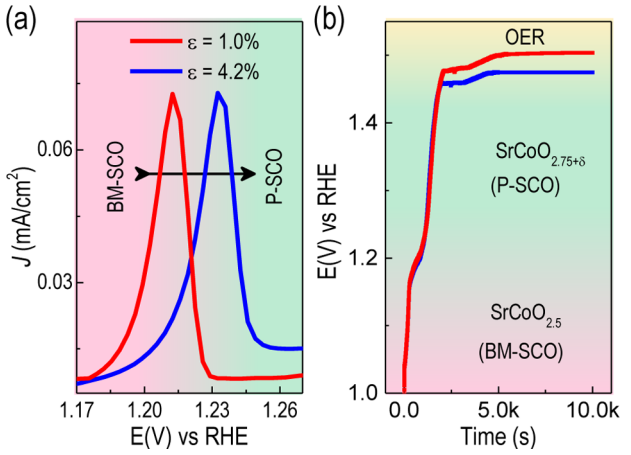

Figure 3. (a) Anodic scan around the topotactic transformation peak as BM-SCO is oxidized to P-SCO. (b) Galvanostatic stability scans at 5 μA for SCO/LSMO on LSAT (ε = 1.0%) and KTO (ε = 4.2%) at 5 mV/s in O_2-saturated 0.1 M KOH.

the ε = 1.0 and 4.2% films for the oxidative BM-SCO ($SrCoO_{2.5}$) to P-SCO ($SrCoO_{2.75}$) topotactic transformation. Films at intermediate strains display shifts intermediate between those for these two strain values. There is an anodic shift with tensile strain in both this peak and additional perovskite oxidation (as can be seen in the full CV in Figure S4). In our previous theoretical work on annealed SCO, density functional theory calculations revealed that such strain raises the ground-state energy of O^{2-} in a potential vacancy site because of a decline in the stabilizing effects of hybridization between the Co 3d and O 2p orbitals with lengthening of the Co−O bond.[9a,18] Here the anodic peak shift signifies that the driving potential to intercalate oxygen into the film rises with growing tensile strain, which facilitates vacancy generation. Galvanostatic measurements at 5 μA (Figure 3b) indicate that less-strained films are more heavily oxidized and that all of the films are stable for an extended period of time.[12] To further verify that the films were chemically stable after testing, XPS measurements were used to compare the Sr/Co composition ratios in P-SCO to BM-SCO (Figure S5). While P-SCO is always enriched in Sr near the surface, there is no statistical difference between the composition of the initially oxidized P-SCO and P-SCO that had undergone OER testing.

Polarization curves for strained P-SCO are shown in Figure 4. Since these oxides are epitaxial films and not in nano-

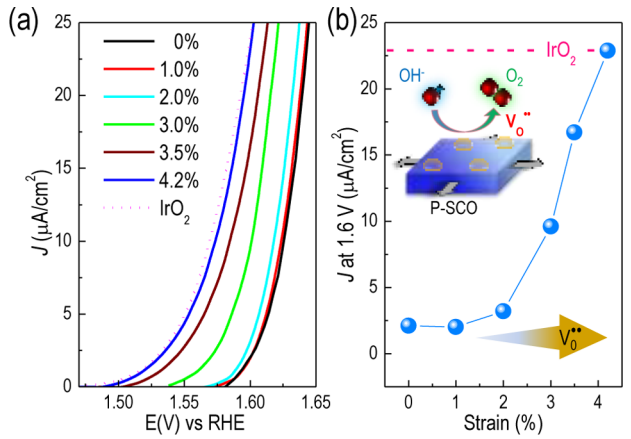

Figure 4. Evolution of OER activity with epitaxial stain: (a) polarization curves for the OER reaction on P-SCO under increasing amounts of biaxial tensile strain; (b) current densities at 1.6 V vs RHE for all of the films are plotted as a function of strain. The activity for a textured (111) IrO_2 film is included.

particulate form within a carbon matrix, it is difficult to directly compare the activities in this study with previous thin-film results.[19] Therefore, a 50 nm thick (111) IrO_2 thin film, representative of a high-activity noble-metal catalyst, was deposited on GC by physical vapor deposition and tested under the same conditions.[20] As the tensile strain in P-SCO is increased from 0 to 4.2%, the onset potential for the OER, as defined by the intersection of the tangents from the linear portion of each curve, is reduced by ~100 mV toward the onset of IrO_2. The inverse relationship between catalytic activity and conductivity (Figure 2a) as well as thickness studies on P-SCO (Figure S6) suggest that here, as opposed to $LaCoO_3$, charge transfer considerations do not hinder the OER reaction.[13] To ensure that the LSMO did not affect the activity, P-SCO/LSMO on the nonconducting STO substrate used throughout this study was also compared to P-SCO on a conducting Nb-doped STO substrate, and only minor differences in activity were found (Figure S5). Furthermore, the Tafel slopes are ~40 mV/dec for all of the strained oxides and IrO_2 films (Figure S7), suggesting a similar reaction mechanism that is enhanced by oxygen nonstoichiometry at the surface.[20,21] Finally, since CV/galvanostatic oxidation measurements indicated that the OER is the dominant reaction at 1.6 V,[6a] we quantitatively compared the activities of these films by observing J at this common OER potential.[12] These activities rose by over an order of magnitude for films containing increased oxygen vacancies via application of modest tensile strain up to ~4% (Figure 4b), becoming comparable to that of IrO_2.[20,22]

In summary, we have established through epitaxially straining of $SrCoO_{3-\delta}$ thin films that oxygen deficiencies in the cobaltite can be tailored from $\delta \leq 0.1$ to $\delta \sim 0.25$ in aqueous, highly oxidizing environments. These shifts in the oxygen content occur through modest amounts of tensile strain over 1%, resulting in anion concentrations not possible before in the unstrained bulk material. This newfound ability to control the

DOI: 10.1021/jacs.6b03520
J. Am. Chem. Soc. 2016, 138, 7252−7255

oxygen vacancy concentration during the OER allows the enhancement of the cobaltite's activity by more than an order of magnitude, commensurate with the catalytic performance of more expensive fully oxidized noble-metal electrodes such as IrO_2. Such an increase in activity is likely due to the vacancies themselves or the resultant increase in Co^{3+}, which in the intermediate spin state can act as an e_g^1 perovskite catalyst as first hypothesized by Suntivich et al.[7] Moreover, this increase in activity is not accompanied by a decrease in structural or chemical stability, as found in other oxides reliant on cation rather than anion substitution.[6a] Consequently, the realization that strain can decouple the traditional relationship between oxygen and electrochemical operating conditions promises new functionalities in metal oxides for energy applications.

■ ASSOCIATED CONTENT

Supporting Information

The Supporting Information is available free of charge on the ACS Publications website at DOI: 10.1021/jacs.6b03520.

Experimental details, XRD θ–2θ scans and RSMs for BM-SCO and P-SCO, electrical transport from 2 to 300 K, CVs of strained films, XPS chemical stability measurements, effects of the LSMO underlayer and P-SCO film thickness on OER activity, and Tafel curves (PDF)

■ AUTHOR INFORMATION

Corresponding Author

*hnlee@ornl.gov

Notes

The authors declare no competing financial interest.

■ ACKNOWLEDGMENTS

This work was supported by the Laboratory Directed Research and Development Program of Oak Ridge National Laboratory, managed by UT-Battelle, LLC, for the U.S. Department of Energy (DOE) (electrochemical characterization) and by the U.S. DOE, Office of Science, Basic Energy Sciences, Materials Science and Engineering Division (synthesis and physical property characterization). Reference electrode depositions were performed as a user project at the Center for Nanophase Materials Sciences, a DOE Office of Science User Facility.

■ REFERENCES

(1) (a) Petrik, N. G.; Zhang, Z.; Du, Y.; Dohnalek, Z.; Lyubinetsky, I.; Kimmel, G. A. *J. Phys. Chem. C* **2009**, *113*, 12407–12411. (b) Wendt, S.; Sprunger, P. T.; Lira, E.; Madsen, G. K. H.; Li, Z.; Hansen, J. Ø.; Matthiesen, J.; Blekinge-Rasmussen, A.; Lægsgaard, E.; Hammer, B.; Besenbacher, F. *Science* **2008**, *320*, 1755–1759. (c) Pena, M. A.; Fierro, J. L. G. *Chem. Rev.* **2001**, *101*, 1981–2018. (d) Esch, F.; Fabris, S.; Zhou, L.; Montini, T.; Africh, C.; Fornasiero, P.; Comelli, G.; Rosei, R. *Science* **2005**, *309*, 752–755. (e) Sayle, D. C.; Sayle, T. X. T.; Parker, S. C.; Catlow, C. R. A.; Harding, J. H. *Phys. Rev. B: Condens. Matter Mater. Phys.* **1994**, *50*, 14498–14505.

(2) (a) Pasierb, P.; Komornicki, S.; Rekas, M. *J. Phys. Chem. Solids* **1999**, *60*, 1835–1844. (b) Kubicek, M.; Cai, Z.; Ma, W.; Yildiz, B.; Hutter, H.; Fleig, J. *ACS Nano* **2013**, *7*, 3276–3286.

(3) Bikondoa, O.; Pang, C. L.; Ithnin, R.; Muryn, C. A.; Onishi, H.; Thornton, G. *Nat. Mater.* **2006**, *5*, 189–192.

(4) Kim, J.; Yin, X.; Tsao, K.-C.; Fang, S.; Yang, H. *J. Am. Chem. Soc.* **2014**, *136*, 14646–14649.

(5) Chang, S. H.; Danilovic, N.; Chang, K.-C.; Subbaraman, R.; Paulikas, A. P.; Fong, D. D.; Highland, M. J.; Baldo, P. M.; Stamenkovic, V. R.; Freeland, J. W.; Eastman, J. A.; Markovic, N. M. *Nat. Commun.* **2014**, *5*, 4191.

(6) (a) Grimaud, A.; May, K. J.; Carlton, C. E.; Lee, Y.-L.; Risch, M.; Hong, W. T.; Zhou, J.; Shao-Horn, Y. *Nat. Commun.* **2013**, *4*, 2439. (b) Bajdich, M.; García-Mota, M.; Vojvodic, A.; Nørskov, J. K.; Bell, A. T. *J. Am. Chem. Soc.* **2013**, *135*, 13521–13530.

(7) Suntivich, J.; May, K. J.; Gasteiger, H. A.; Goodenough, J. B.; Shao-Horn, Y. *Science* **2011**, *334*, 1383–1385.

(8) (a) Kalinin, S. V.; Spaldin, N. A. *Science* **2013**, *341*, 858–859. (b) Mannhart, J.; Schlom, D. G. *Nature* **2004**, *430*, 620–621. (c) Campbell, C. T.; Peden, C. H. F. *Science* **2005**, *309*, 713–714. (d) Chen, D.; Chen, C.; Baiyee, Z. M.; Shao, Z.; Ciucci, F. *Chem. Rev.* **2015**, *115*, 9869–9921.

(9) (a) Petrie, J. R.; Mitra, C.; Jeen, H.; Choi, W. S.; Meyer, T. L.; Reboredo, F. A.; Freeland, J. W.; Eres, G.; Lee, H. N. *Adv. Funct. Mater.* **2016**, *26*, 1564–1570. (b) Choi, W. S.; Jeen, H.; Lee, J. H.; Seo, S. S. A.; Cooper, V. R.; Rabe, K. M.; Lee, H. N. *Phys. Rev. Lett.* **2013**, *111*, 097401. (c) Jeen, H.; Choi, W. S.; Biegalski, M. D.; Folkman, C. M.; Tung, I. C.; Fong, D. D.; Freeland, J. W.; Shin, D.; Ohta, H.; Chisholm, M. F.; Lee, H. N. *Nat. Mater.* **2013**, *12*, 1057–1063.

(10) Mitra, C.; Meyer, T.; Lee, H. N.; Reboredo, F. A. *J. Chem. Phys.* **2014**, *141*, 084710.

(11) Katsounaros, I.; Cherevko, S.; Zeradjanin, A. R.; Mayrhofer, K. J. J. *Angew. Chem., Int. Ed.* **2014**, *53*, 102–121.

(12) Nemudry, A.; Rudolf, P.; Schoellhorn, R. *Chem. Mater.* **1996**, *8*, 2232.

(13) Risch, M.; Stoerzinger, K. A.; Maruyama, S.; Hong, W. T.; Takeuchi, I.; Shao-Horn, Y. *J. Am. Chem. Soc.* **2014**, *136*, 5229–5232.

(14) Lu, X.; Yim, W.-L.; Suryanto, B. H. R.; Zhao, C. *J. Am. Chem. Soc.* **2015**, *137*, 2901–2907.

(15) Le Toquin, R.; Paulus, W.; Cousson, A.; Prestipino, C.; Lamberti, C. *J. Am. Chem. Soc.* **2006**, *128*, 13161.

(16) (a) Aschauer, U.; Pfenninger, R.; Selbach, S. M.; Grande, T.; Spaldin, N. A. *Phys. Rev. B: Condens. Matter Mater. Phys.* **2013**, *88*, 054111. (b) Chen; Yu; Adler, S. B. *Chem. Mater.* **2005**, *17*, 4537–4546.

(17) (a) Balamurugan, S.; Yamaura, K.; Karki, A. B.; Young, D. P.; Arai, M.; Takayama-Muromachi, E. *Phys. Rev. B: Condens. Matter Mater. Phys.* **2006**, *74*, 172406. (b) Kuneš, J.; Křápek, V.; Parragh, N.; Sangiovanni, G.; Toschi, A.; Kozhevnikov, A. V. *Phys. Rev. Lett.* **2012**, *109*, 117206.

(18) Kushima, A.; Yip, S.; Yildiz, B. *Phys. Rev. B: Condens. Matter Mater. Phys.* **2010**, *82*, 115435.

(19) Suntivich, J.; Gasteiger, H. A.; Yabuuchi, N.; Shao-Horn, Y. *J. Electrochem. Soc.* **2010**, *157*, B1263–B1268.

(20) Stoerzinger, K. A.; Qiao, L.; Biegalski, M. D.; Shao-Horn, Y. *J. Phys. Chem. Lett.* **2014**, *5*, 1636–1641.

(21) Hardin, W. G.; Mefford, J. T.; Slanac, D. A.; Patel, B. B.; Wang, X.; Dai, S.; Zhao, X.; Ruoff, R. S.; Johnston, K. P.; Stevenson, K. J. *Chem. Mater.* **2014**, *26*, 3368–3376.

(22) Damjanovic, A.; Dey, A.; Bockris, J. O. M. *J. Electrochem. Soc.* **1966**, *113*, 739–746.

DOI: 10.1021/jacs.6b03520
J. Am. Chem. Soc. 2016, 138, 7252–7255